THE JOURNAL OF CHEMICAL PHYSICS **146**, 044306 (2017)

Structures and electronic properties of $B_3Si_n^-$ (n = 4–10) clusters: A combined *ab initio* and experimental study

Xue Wu,[1] Sheng-Jie Lu,[2,3] Xiaoqing Liang,[1] Xiaoming Huang,[4] Ying Qin,[1] Maodu Chen,[1] Jijun Zhao,[1,a)] Hong-Guang Xu,[2,3,b)] R. Bruce King,[5] and Weijun Zheng[2,3]
[1]*Key Laboratory of Materials Modification by Laser, Ion and Electron Beams (Dalian University of Technology), Ministry of Education, Dalian 116024, China*
[2]*Beijing National Laboratory for Molecular Sciences, State Key Laboratory of Molecular Reaction Dynamics, Institute of Chemistry, Chinese Academy of Sciences, Beijing 100190, China*
[3]*University of Chinese Academy of Sciences, Beijing 100049, People's Republic of China*
[4]*School of Ocean Science and Technology, Dalian University of Technology, Panjin Campus, Panjin 124221, China*
[5]*Department of Chemistry and Center for Computational Chemistry, University of Georgia, Athens, Georgia 30602, USA*

(Received 28 October 2016; accepted 7 January 2017; published online 25 January 2017)

The anionic silicon clusters doped with three boron atoms, $B_3Si_n^-$ (n = 4–10), have been generated by laser vaporization and investigated by anion photoelectron spectroscopy. The vertical detachment energies (VDEs) and adiabatic detachment energies (ADEs) of these anionic clusters are determined. The lowest energy structures of $B_3Si_n^-$ (n = 4–10) clusters are globally searched using genetic algorithm incorporated with density functional theory (DFT) calculations. The photoelectron spectra, VDEs, ADEs of these $B_3Si_n^-$ clusters (n = 4–10) are simulated using B3LYP/6-311+G(d) calculations. Satisfactory agreement is found between theory and experiment. Most of the lowest-energy structures of $B_3Si_n^-$ (n = 4–10) clusters can be derived by using the squashed pentagonal bipyramid structure of $B_3Si_4^-$ as the major building unit. Analyses of natural charge populations show that the boron atoms always possess negative charges, and that the electrons transfer from the 3*s* orbital of silicon and the 2*s* orbital of boron to the 2*p* orbital of boron. The calculated average binding energies, second-order differences of energies, and the HOMO-LUMO gaps show that $B_3Si_6^-$ and $B_3Si_9^-$ clusters have relatively high stability and enhanced chemical inertness. In particular, the $B_3Si_9^-$ cluster with high symmetry (C_{3v}) stands out as an interesting superatom cluster with a magic number of 40 skeletal electrons and a closed-shell electronic configuration of $1S^21P^61D^{10}2S^22P^61F^{14}$ for superatom orbitals. *Published by AIP Publishing.* [http://dx.doi.org/10.1063/1.4974337]

I. INTRODUCTION

Silicon has been the most important material in microelectronics and semiconductor industry for many years. The increasing miniaturization of silicon-based transistors has led to considerable efforts devoted to the fundamental understanding of silicon clusters. Unlike carbon, whose small clusters tend to form linear or planar cyclic structures with sp^2 hybridization, bare silicon clusters favor sp^3-like bonding and three-dimensional structures.[1–7] Both density functional theory (DFT) calculations[8–15] and experiments[16–21] showed that doping metal atoms into silicon clusters can enhance the stability and modify the geometries and physical properties of the silicon clusters. This provides new opportunities in microelectronics and spintronics. The silicon clusters doped with non-metallic elements like boron also attract great attention.

In the bulk phase, boron-silicon alloys are semiconductors useful for applied materials science such as power transistors.[22] Implanting boron atoms into silicon materials leads to some novel physical properties and devices such as Si-based ultrashallow junctions.[23] Very high dose ion implantation creates a low-resistivity region,[24] and deep boron ion implantation leads to significant electrical activity.[25] Implanting boron clusters in silicon crystals has been studied by X-ray photoelectron spectroscopy.[26,27] However, ion implantation is known to damage the crystalline structure of silicon and to create an amorphous zone close to the irradiated surface.[28]

Inspired by the studies of bulk boron-silicon alloys, the geometric structures and thermochemical parameters of boron doped silicon clusters have been investigated both theoretically[29–35] and experimentally.[36,37] In an early calculation, Boldyrev and Simons predicted BSi dimer to have a high-spin ground electronic state.[29] Their result was subsequently confirmed experimentally by Knight *et al.*[36] The small boron-silicon clusters, such as SiB_2, Si_2B, and Si_2B_2, tend to form rings with strong π-bonding interactions rather than open chains.[30] Recently, Ueno *et al.* found small boron-silicon and boron-germanium clusters up to 4 atoms to possess similar structures.[31] Interestingly, Ngan and Nguyen rationalized the existence of cubic silicon clusters by doping M (M = Be, B, and C^+) at the center of a Si_8 cube.[32] Very recently, Si_6B was studied by Truong *et al.* using infrared spectroscopy.[37] Some theoretical studies have been devoted to the thermochemical parameters and growth mechanisms of B-doped silicon clusters.[33–35] These studies reveal that planar structures are

---

[a)] Electronic mail: zhaojj@dlut.edu.cn
[b)] Electronic mail: xuhong@iccas.ac.cn

dominant for small B_nSi clusters with $n < 6$ and that each Si_nB cluster is formed by adding an excess Si atom to $Si_{n-1}B$ rather than adding B into Si_n. Photoelectron spectroscopy and *ab initio* calculations on $B_2Si_6^{-/0/+}$ show that their structures can be characterized as a Si atom hanging over a distorted bowl-like B_2Si_5 framework.[38]

Despite the studies mentioned above, our knowledge on mixed silicon-boron clusters remains rather limited. In particular, silicon clusters doped with more than two boron atoms have not been explored yet. Therefore, a systematic investigation on $B_3Si_n^-$ clusters appears necessary to gain more insights into the structural features and fundamental properties of these intriguing systems. In this paper, we describe a combined study of DFT calculations and experimental photoelectron spectroscopy on $B_3Si_n^-$ clusters with n = 4–10. Among them, we find that the closed-shell system $B_3Si_9^-$ has an enhanced stability with a magic number of 40 skeletal electrons and a molecular orbital configuration of $1S^2 1P^6 1D^{10} 2S^2 2P^6 1F^{14}$.

II. EXPERIMENTAL AND THEORETICAL

A. Experimental

The experiments were conducted using a home-built apparatus consisting of a laser vaporization cluster source, a time-of-flight mass spectrometer, and a magnetic-bottle photoelectron spectrometer, which have been described elsewhere.[17] The B–Si cluster anions were generated in the laser vaporization source by laser ablation of a rotating and translating disk target (13 mm diameter, B:Si mole ratio 1:1) with the second harmonic (532 nm) light pulses from a Nd:YAG laser (Continuum Surelite II-10). Helium gas with ∼5 atm backing pressure was allowed to expand through a pulsed valve (General Valve Series 9) into the source to cool the formed clusters. The generated cluster anions were mass-analyzed with the time-of-flight mass spectrometer. The cluster anions of interest were size-selected with a mass gate, decelerated by a momentum decelerator before crossed by the laser beam of another Nd:YAG laser (Continuum Surelite II-10, 266 nm) at the photodetachment region. The photoelectrons were energy-analyzed by the magnetic-bottle photoelectron spectrometer. The photoelectron spectra were calibrated using the spectra of Cu^- and Au^- anions taken at the similar conditions. The resolution of the magnetic-bottle photoelectron spectrometer was about 40 meV at an electron kinetic energy of 1 eV.

B. Theoretical

The lowest energy $B_3Si_n^-$ (n = 4–10) cluster anion structures were globally searched using our own comprehensive genetic algorithm (CGA) code[15] incorporated with DFT calculations (CGA-DFT). Further details of CGA can be found in a recent review article.[15] As one of the most widely adopted global optimization algorithms, GA and its variations have been intensively used in cluster science.[39,40] The validity and efficiency of the present CGA-DFT scheme have been well demonstrated in our previous studies on Ga_n,[41] Na_n,[42] Ca_n,[43] Na–Si,[13] V–Si,[14,44] $(WO_3)_n$,[45] Pt–Sn,[46] and Au–Ag[47] clusters. As a successful application, the most stable configurations of neutral and anionic Na_nSi_m (n = 1–3 and m = 1–11) clusters were obtained. The theoretical electronic properties were found to compare well with experimental data.[13]

All cluster structures were fully relaxed by DFT calculations without any symmetry constraint. The double numerical basis including *d*-polarization function (DND) and the Perdew-Burke-Enzerhof (PBE) functional within the generalized gradient approximation (GGA),[48] as implemented in the DMol^3 program,[49,50] were adopted. For comparison, we also optimized all cluster structures at the B3LYP/6-311+G(d)[51,52] level using the Gaussian 09 program.[53] The results from the B3LYP/6-311+G(d) method were found to be in slightly better agreement with the experiment than the PBE/DND results. Therefore, the former approach was employed to simulate the photoelectron spectra of the $B_3Si_n^-$ (n = 4–10) cluster anions using the configurations from the CGA-DFT global search.

The accuracy of the B3LYP/6-311+G(d) methodology was assessed by benchmark calculations on B_2 and Si_2 dimers as well as previous theoretical and experimental work.[30,54] The calculated B–B bond length (BL) of B_2 dimer is 1.641 Å and is in good agreement with the previous theoretical value of 1.589 Å.[30] Similarly, the theoretical Si–Si BL of 2.307 Å of Si_2 is comparable to the experimental value 2.246 Å.[54]

The PB functional[55,56] combined with the DND basis set was also used to compute the vibrational frequencies of different isomers of $B_3Si_n^-$ (n = 4–10) clusters. These were then used to derive free energy at finite temperatures and zero-point vibrational energies. The natural population analysis (NPA) of $B_3Si_n^-$ was conducted using the Natural Bond Orbital (NBO) 3.1 program[57–61] implemented in the Gaussian 09 package.

III. RESULTS AND DISCUSSION

A. Photoelectron spectra of $B_3Si_n^-$ (n = 4–10) clusters

The photoelectron spectra of $B_3Si_n^-$ (n = 4–10) clusters recorded with 266 nm photons are presented in Fig. 1. Note that the original photoelectron spectrum of $B_3Si_9^-$ has some contamination from the signals of Si_{10}^- because the mass peaks of $B_3Si_9^-$ overlap with the strong mass peaks of Si_{10}^-. The photoelectron spectrum of $B_3Si_9^-$ shown in Fig. 1 is acquired by subtracting the signals of Si_{10}^- from the original spectrum (details in the supplementary material Table SI). Analogous contamination in the other $B_3Si_n^-$ ($n \neq 9$) spectra can be ignored because the mass peaks of Si_m^- ($m \neq 10$) are weak. From the measured spectra, the vertical detachment energies (VDEs) can be determined from the peak maxima of the first photoelectron spectra feature. The adiabatic detachment energies (ADEs) can be determined from the leading edge of the first peak. By definition, the VDE is the transition energy from the ground state of a cluster anion to the neutral ground state at same nuclear configuration, and ADE (also known as the electron affinity) is the difference in total energy between the optimized geometries of the anion and neutral clusters. Owing to the absence of resolved vibrational structures in the experimental spectra, the ADE cannot be determined accurately.[62] Thus here we only discuss VDEs.

Many peaks in the spectra of $B_3Si_n^-$ (n = 4–9) clusters can be distinguished. The spectrum of $B_3Si_4^-$ shows three

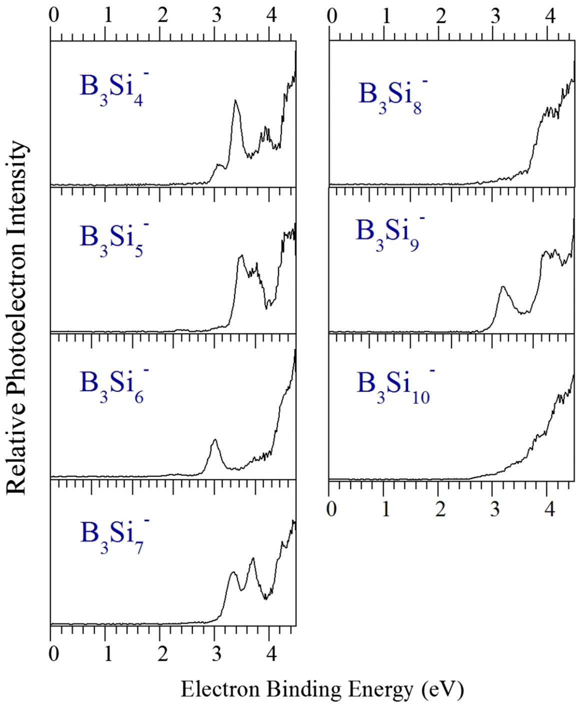

FIG. 1. Photoelectron spectra of $B_3Si_n^-$ (n = 4–10) clusters recorded with 266 nm photons.

major peaks centered at 3.09, 3.38, and 3.93 eV as well as the onset of a broad peak above 4.2 eV. The spectrum of $B_3Si_5^-$ has two overlapping peaks centered at 3.48 and 3.75 eV and another broad peak above 4.1 eV. The spectrum of $B_3Si_6^-$ has one major peak centered at 3.00 eV and another broad peak higher than 4.0 eV. The spectrum of $B_3Si_7^-$ has two peaks centered at 3.34 and 3.71 eV and some unresolved strong peaks above 4.1 eV. The spectral features of $B_3Si_8^-$ are rather broad. We can barely distinguish two peaks: one is in the range of 3.6–4.2 eV and the other is above 4.2 eV. The spectrum of $B_3Si_9^-$ has a resolved peak centered at 3.19 eV, followed by two barely resolved peaks centered at 3.97 and 4.15 eV, and another one above 4.3 eV. In the spectrum of $B_3Si_{10}^-$, the spectral features extend from ~3.0 eV to the end of the x-axis. Almost no spectral feature can be resolved except that some steps can be observed at about 3.35, 3.83, and 4.22 eV. The VDEs and ADEs of the cluster anions measured from the photoelectron spectra are listed in Table I.

B. Low-energy structures of $B_3Si_n^-$ (n = 4–10) clusters

The potential energy surfaces of $B_3Si_n^-$ (n = 4–10) cluster anions were explored in an unbiased manner using CGA-DFT calculations. For each size, the ground state configuration along with several low-lying isomers was obtained. Their photoelectron spectra were simulated using the generalized Koopman theorem,[63,64] in which each transition corresponds to the removal of an electron from a specific molecular orbital of the cluster anion. The representative low-lying isomers of $B_3Si_n^-$ (n = 4–10) after DFT optimization are presented in Fig. 2. The lowest energy structures are designated as nA (n = 4–10). The relative energies between these isomers as well as their theoretical VDEs and ADEs are summarized in Table I. To facilitate comparison with experimental spectra, we integrated the simulated spectra and the experimental photoelectron spectra in Fig. 3.

1. $B_3Si_4^-$

As shown in Fig. 2, $B_3Si_4^-$ has two low-energy isomers (4A and 4B). The lowest energy $B_3Si_4^-$ structure (4A) is a squashed pentagonal bipyramid with C_s symmetry, in which the three boron atoms form an acute triangle. The stability of the ground-state 4A configuration can be rationalized by the Wade-Mingos rules[65,66] which were originally derived to relate the structures of polyhedral boranes to the number of skeletal electrons. According to the Wade-Mingos rules, a closo deltahedral structure with n vertices requires 2n + 2 electrons for skeletal bonding. Thus the 7-vertex 4A cluster requires 16 skeletal electrons for a closo deltahedral structure, namely, the pentagonal bipyramid. However, the total number of valence electrons in 4A is 26, with three boron atoms providing 9 valence electrons and four silicon atoms providing 16 electrons and the extra electron obtained from reduction to the monoanion. This leaves 10 remaining electrons to form 5 external lone pairs on the equatorial atoms. The special stability of 4A can be also ascribed to three-dimensional aromaticity.[67–69] Note that the 7-vertex pentagonal bipyramid is the smallest deltahedron that meets the requirements of an oblatocloso deltahedron. Previously, King *et al.* studied the 7-vertex oblatocloso deltahedron identical to the structure of 4A.[70] More importantly, the squashed pentagonal bipyramidal 4A configuration is an important structural unit for building many low-energy larger $B_3Si_n^-$ cluster structures, as we will show later.

The metastable 4B $B_3Si_4^-$ isomer, which is 0.08 eV higher in energy, has a central B_3Si tetrahedron with three B_2Si faces capped by the three remaining silicon atoms. The calculated VDEs of both 4A (3.27 eV) and 4B (3.32 eV) are in reasonable agreement with the experimental value (3.09 eV). As seen in Fig. 3, the simulated spectrum of 4A shows four discrete peaks and agrees well with the experimental photoelectron spectrum, except the second one. In contrast to 4A, 4B only shows two discrete peaks that coincide with the first two peaks in the measured spectrum. Therefore, it is very likely that 4A and 4B isomers coexist in the cluster beam in the experiment.

2. $B_3Si_5^-$

For $B_3Si_5^-$ cluster, we found four low-lying isomers (5A, 5B, 5C, and 5D). The C_s $B_3Si_5^-$ isomer 5A is derived from the $B_3Si_4^-$ isomer 4A by capping one of the SiB_2 faces with the fifth silicon atom. The $B_3Si_5^-$ isomers 5B, 5C, and 5D are higher energy structures, lying 0.91, 0.92, and 1.20 eV, respectively, in energy above 5A. The $B_3Si_5^-$ isomer 5B can be described as an Si_5 pentagon capped on one side by a boron atom and on the other side by a B_2 dimer. The $B_3Si_5^-$ isomer 5C can be considered as a B_3Si_4 pentagonal bipyramid with the fifth silicon atom capping an Si_2B face. The boron atoms in 5C form an obtuse triangle, different from the other low-energy $B_3Si_5^-$ isomers. The computed VDEs of 5A, 5B, and 5C are 3.39, 3.08, and 2.92 eV, respectively. Among them, the VDE of 5A coincides with the experimental value (3.48 eV) well. Since the VDE of 5D is notably less stable than 5A, it is also unlikely to be detected in the experiment. From Fig. 3, we can see that

TABLE I. Experimental and theoretical vertical detachment energies (VDEs) and adiabatic detachment energies (ADEs) as well as theoretical HOMO-LUMO gaps (E_{HL}) of $B_3Si_n^-$ clusters. All quantities are in the unit of eV. The uncertainties in the last digits of the experimental VDEs and ADEs are shown in the parentheses.

				VDE(eV)		ADE(eV)	
	Isomers	ΔE(eV)	E_{HL}(eV)	Theo.	Expt.	Theo.	Expt.
$B_3Si_4^-$	4A	0	3.35	3.27	3.09 (8)	3.07	2.92 (8)
	4B	0.08	2.56	3.32		3.09	
$B_3Si_5^-$	5A	0	3.01	3.39	3.48 (8)	3.17	3.27 (8)
	5B	0.91	3.02	3.08		2.89	
	5C	0.92	2.63	2.92		2.66	
	5D	1.20	2.18	2.89		2.75	
$B_3Si_6^-$	6A	0	2.17	2.81	3.00 (8)	2.64	2.78 (8)
	6B	0.24	2.65	3.13		2.97	
$B_3Si_7^-$	7A	0	3.06	3.33	3.34 (8)	3.01	3.06 (8)
	7B	0.086	2.79	3.13		2.91	
	7C	0.089	2.79	3.21		2.99	
	7D	0.16	2.88	3.18		3.01	
$B_3Si_8^-$	8A	0	3.39	3.80	3.9 (2)	3.50	3.7 (2)
	8B	0.09	3.28	3.68		3.36	
$B_3Si_9^-$	9A	0	3.18	3.09	3.19 (8)	3.00	2.95 (8)
	9B	0.27	2.85	3.30		2.96	
	9C	0.46	2.48	3.25		3.07	
	9D	0.54	2.29	3.13		2.96	
	9E	0.56	1.36	3.23		2.86	
$B_3Si_{10}^-$	10A	0	2.54	3.51	3.4 (2)	3.16	3.2 (2)
	10B	0.027	2.46	3.47		3.13	
	10C	0.031	2.73	3.40		3.02	
	10D	0.17	2.62	3.19		3.19	
	10E	0.38	2.68	3.27		3.05	

the simulated spectrum of 5A shows two peaks. Even though its VDE agrees well with the experimental value, the number of spectral peaks is less than that in the experiment. Therefore, some features in the experimental photoelectron spectrum of $B_3Si_5^-$ cannot be matched by the simulated spectrum of isomer 5A alone and might originate from other isomers such as 5B.

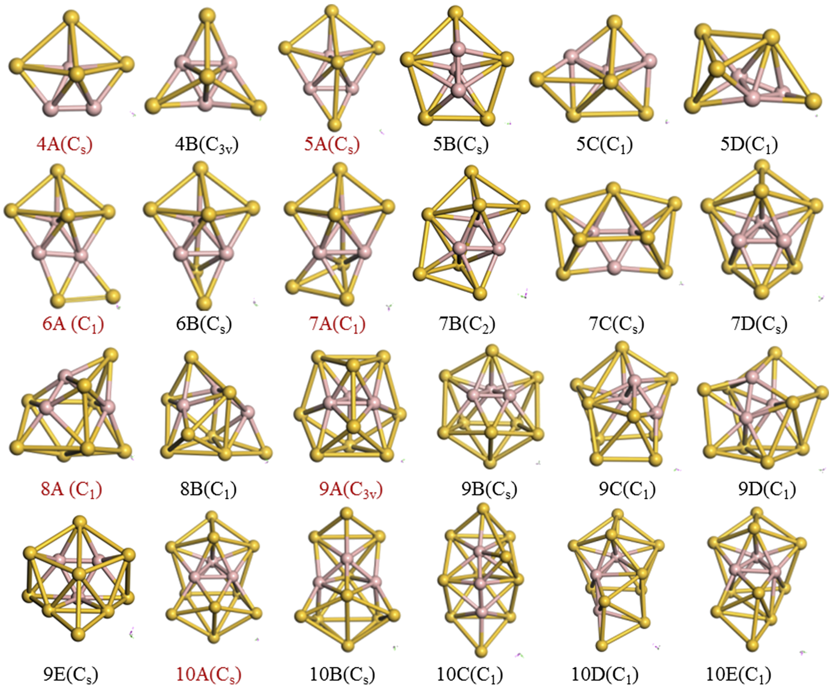
4A(C_s) 4B(C_{3v}) 5A(C_s) 5B(C_s) 5C(C_1) 5D(C_1)

6A (C_1) 6B(C_s) 7A(C_1) 7B(C_2) 7C(C_s) 7D(C_s)

8A (C_1) 8B(C_1) 9A(C_{3v}) 9B(C_s) 9C(C_1) 9D(C_1)

9E(C_s) 10A(C_s) 10B(C_s) 10C(C_1) 10D(C_1) 10E(C_1)

FIG. 2. Low-energy structures of $B_3Si_n^-$ (n = 4–10) clusters. For each cluster size n, the energy difference of several isomers (marked as nA, nB, nC, and so on) with regard to the lowest-energy one (marked as nA). The cluster symmetries and energy differences (ΔE) are given in brackets and the second row, respectively. Yellow and lilac balls represent Si and B atoms, respectively.

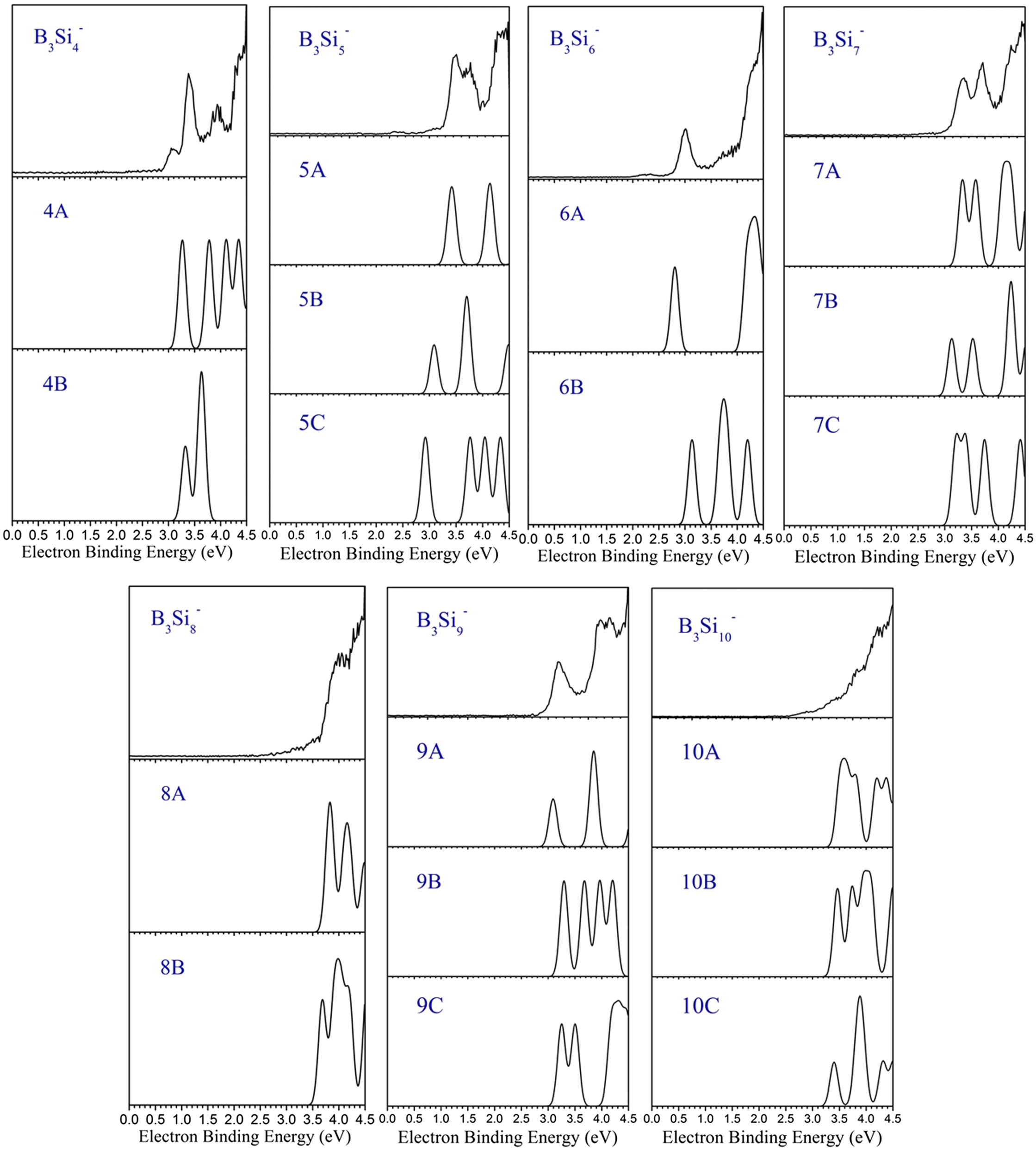

FIG. 3. Comparison between the experimental photoelectron spectra and the simulated photoelectron spectra of the low-lying isomers of $B_3Si_n^-$ (n = 4–10) clusters. The simulations were conducted by fitting the distribution of the transition lines with unit-area Gaussian functions of 0.075 eV broadening.

3. $B_3Si_6^-$

The two lowest-energy $B_3Si_6^-$ isomers 6A and 6B have similar energies with 6B lying only 0.24 eV above 6A. Both of them can be described as a central squashed pentagonal bipyramid with two external atoms. The 6A structure is obtained by adding two silicon atoms to the B–B bond of pentagon. Isomer 6B with C_s symmetry can be derived by capping two additional silicon atoms on the triangular facet of B_3. The VDEs of $B_3Si_6^-$ isomer are 2.81 eV (6A) and 3.13 eV (6B), respectively, which are also comparable to our experiment value of 3.00 eV. From Fig. 3, we can see that the simulated spectrum of 6A shows a sharp lowest-energy peak at 2.81 eV with a small shift of ~0.2 eV compared to the experimental data. The next peak agrees well with the experiment spectrum. The three discrete peaks in 6B, however, disagree with the experimental feature. Hence, we suggest that isomer 6A is the most probable structure detected in the experiment.

4. $B_3Si_7^-$

Our calculations show that the first three isomers of $B_3Si_7^-$ isomers, namely, 7A, 7B, and 7C, to be nearly degenerate on the potential energy surface, with energy difference less than 0.1 eV. The ground state configuration of 7A is obtained by capping one silicon atom on the bottom of 6B. The C_2 $B_3Si_7^-$ isomer 7B can be described as two pentagonal bipyramidal B_3Si_4 structural units spliced together by sharing three boron atoms and one silicon atom. The structure of 7C is not based on the pentagonal bipyramid like most of the other B_3Si_n ($n = 4, 5, 6, 7$) structures. Instead it can be viewed as a severely distorted octahedron capped by Si_2 dimers on the two opposite sides. 7D is a bicapped square antiprism with silicon atoms at the degree 4 capping vertices.

The VDEs of these four $B_3Si_7^-$ isomers 7A, 7B, 7C, and 7D are 3.33, 3.13, 3.21, and 3.18 eV, respectively. There are three peaks in the simulated spectrum of 7A. The first two overlap with each other, and the first peak at 3.33 eV is very close to the first peak of the experimental photoelectron spectrum of $B_3Si_7^-$; the third peak of the simulated spectrum emerges at 4.16 eV. For 7B, the three peaks centered at 3.13, 3.52, and 4.24 eV are also consistent with the experimental spectrum. The simulated spectrum of 7C looks like that of 7A but with one more peak. Generally speaking, the simulated photoelectron spectra of isomers 7A and 7B are in good agreement with the experiment spectrum of $B_3Si_7^-$. Owing to their small energy difference (only 0.086 eV at 0 K), we speculate that 7A and 7B isomers of $B_3Si_7^-$ may coexist under the experimental conditions.

5. $B_3Si_8^-$

The two isomers obtained here (i.e., 8A and 8B) have irregular shape with no symmetry at all. If we considered a B_3Si_5 square antiprism as structural motif, 8A is obtained by adding three silicon atoms on vertices of B_3Si_5. On the other hand, 8B can be regarded as a mirror image of 8A with some distortion. The simulated VDEs of $B_3Si_8^-$ are 3.80 (8A) and 3.68 eV (8B), respectively, in reasonable agreement with the experimental value (3.9 eV). The simulated spectrum of 8A has three peaks located at 3.83, 4.16, and 4.35 eV, respectively. The first peak is relatively narrow, while the following two peaks overlap and form a shoulder. For 8B, the first peak appears at 3.68 eV and overlaps with the second peak then followed by the third peak as the shoulder of the second one. The energy difference between 8A and 8B is rather small, only 0.09 eV. Thus, it is possible for 8A and 8B to coexist in the cluster beam in the experiment. The overlapping of the peaks of 8A and 8B can explain why the experimental spectral features of $B_3Si_8^-$ are very broad.

6. $B_3Si_9^-$

Again, $B_3Si_9^-$ does not follow the structural motif of $B_3Si_4^-$. Among the first five isomers, 9A with C_{3v} symmetry is particularly interesting. It has a waist-capped 3-3-3 layered structure: a Si_3 triangle as the top layer, a B_3 triangle as the intermediate layer, a Si_3 triangle as the bottom layer, and three additional Si atoms capped on the waist between the middle and bottom layers. In another view of 9A, nine silicon atoms form three equivalent interlocking pentagons. Each boron atom occupies the center of one of these three Si_5 pentagons. Structure 9A can thus be derived from a $B_3Si_9^-$ icosahedron with three equivalent boron vertices by squeezing the boron vertices towards the center to form a bonded B_3 triangle inside the icosahedron. Structure 9B is also a distorted icosahedron lying 0.27 eV above 9A. Isomer 9C is composed of two interpenetrating pentagonal pyramids by sharing three edge Si atoms. Isomer 9D has a central twisted BSi_9 pentagonal prism with the two remaining boron atoms capping the pentagonal faces. The $B_3Si_9^-$ isomers 9A, 9B, and 9D all have nearly planar BSi_5 boron-centered pentagons. Isomers 9C, 9D, and 9E are far less stable than 9A × 0.46, 0.54, and 0.56 eV, respectively. The computed VDEs of various isomers of $B_3Si_9^-$ are 3.09 (9A), 3.30 (9B), 3.25 (9C), 3.13 (9D), and 3.23 eV (9E), respectively. The simulated spectrum of 9A shows two peaks. The first peak located at 3.09 eV is in good agreement with the experiment spectrum, and the following peak located at 3.85 eV is which is slightly lower than the electron binding energy of the nearest experimental peak. For 9B, however, it shows four overlapping peaks, inconsistent with the experimental spectrum. Similarly, 9C displays three main peaks with the first two peaks overlapping with each other. We therefore suspect 9A to be the most probable structure detected in experiments.

7. $B_3Si_{10}^-$

There are five isomers of $B_3Si_{10}^-$ determined from the CGA-DFT global search. As the ground state, the 10A geometry with C_s symmetry is formed by fusion of a B_3Si_4 pentagonal bipyramid to a B_3Si_6 tricapped trigonal prism by sharing a B_3 triangle. The isomers 10B, 10C, and 10D do not follow the structural motif of $B_3Si_4^-$. The 10B configuration with C_s symmetry can be viewed as a layered structure: a pentagonal pyramid on the bottom, a B_3Si quadrangle as the intermediate layer, and a Si_3 triangle as the top layer. The isomers 10C and 10D have no symmetry at all, with three B atoms in axis form. The structure of 10E is related to 10A but the bottom with severe distortion. Isomers 10B, 10C, 10D, and 10E are less stable than isomer 10A × 0.027, 0.031, 0.17, and 0.38 eV, respectively. The VDEs of 10A, 10B, and 10C are 3.51, 3.47, and 3.40 eV, respectively; all of them are in accordance with our experiment value (3.4 eV). The VDEs of the other two isomers (10D and 10E) deviate substantially from the experimental data; it is unlikely for them to be found in the experiment. The simulated spectrum of 10A shows four peaks. The first high intensity peak is located at 3.51 eV, followed by a shoulder peak at 3.85 eV and two closely-spaced peaks at 4.20 and 4.38 eV. 10B displays three main peaks located at 3.47, 3.82, and 4.00 eV, respectively, whereas the latter two peaks overlap with each other. In addition, the fourth peak beyond 4.50 eV is observed. 10C has one high-intensity peak and two low-intensity peaks at 3.40, 3.80, and 4.34 eV, respectively. Isomers 10B and 10C are higher in energy than 10A by only 0.027 and 0.031 eV, respectively. Thus, isomers 10A, 10B, and 10C can coexist in the experiment. This result explains the broad feature of the spectrum of $B_3Si_{10}^-$.

In all, in the low-energy structures of $B_3Si_n^-$ (n = 4–10) clusters, boron atoms tend to bond with each other and form B_3 triangle. The 4A structure obeying the Wade-Mingos rules serves as a constitutional unit to build some $B_3Si_n^-$ cluster structures. Thus the 5A, 6A, 6B, 7A, 7B, 7D, and 10A structures can be obtained by adding Si atoms to 4A. Generally speaking, the $B_3Si_n^-$ systems with 7 to 9 vertices have central squashed pentagonal bipyramid. However, the $B_3Si_n^-$ systems with 10 to 13 vertices are deltahedra containing internal or partially internal bonded B_3 triangles. In general, boron vertices tend to occupy at the sites of relatively low curvature or even negative curvature, and B atoms adsorbed on small silicon clusters prefer to occupy the low-coordination site.

For all the clusters, the comparison of the simulated spectra and experimental photoelectron spectra show satisfactory agreement for the lowest energy isomers, indicating that our *ab initio* global search has found the cluster structures detected in the experiment. Besides, it can be seen that the experimental photoelectron spectra features become broad upon increasing the cluster size. This is a consequence not only of the limited experimental resolution but also due to the coexistence of more than one isomer of comparable energies at experiment temperature.

The measured and computed VDEs and ADEs of the cluster anions are plotted in Fig. 4. Generally, the theoretical VDEs reproduce the experimental data well, while the discrepancy between theoretical and experimental ADEs is slightly larger (~0.14 eV). The local minima at $B_3Si_6^-$ and $B_3Si_9^-$ with regard to its neighboring sizes are found in both ADE and VDE curves. Therefore, from both geometric and electronic points of view, $B_3Si_9^-$ stands out as a unique species with high symmetry and appreciable stability. A detailed analysis of $B_3Si_9^-$ as a superatom cluster will be given in Section III D.

Since the experimental photoelectron spectra were recorded at finite temperature and the first-principles results correspond to zero temperature, the sequence of cluster isomers might be affected by temperature effect, which would in turn influence the photoelectron spectra of a cluster anion. In this regard, we computed the free energies of the isomers of $B_3Si_n^-$ (n = 4–10) cluster with inclusion of vibrational entropy and the zero-point energy.

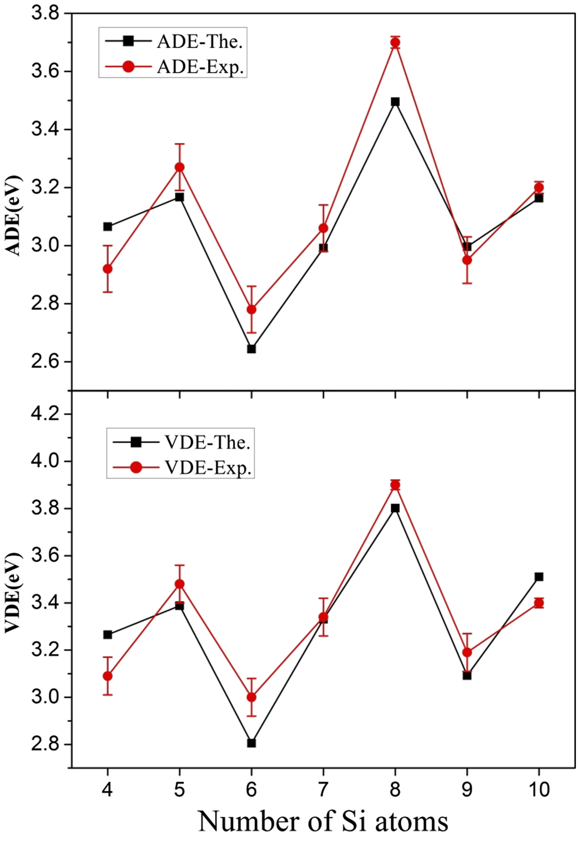

FIG. 4. Vertical detachment energy (VDE) and adiabatic detachment energy (ADE) of the lowest-energy structure of $B_3Si_n^-$ as a function the number of Si atoms. Black squares: theory; red circles with error bars: experiment.

The free energy difference between the ground state configuration and a metastable isomer is defined as follows:

$$E_F(nA - nX) = E_F(nA) - E_F(nX)(n = 4\text{–}10, \quad X = B, C, D \text{ and } E), \tag{1}$$

where $E_F(nA)$ and $E_F(nX)$ are the free energies of the ground state and metastable isomer, respectively. The results are shown in the supplementary material as Fig. S1. For some cluster isomers (6A and 6B, 7A and 7D, 8A and 8B), the free energy difference decreases with temperature. This means that the ground state configuration becomes more and more stable upon increasing the temperature, and that it is impossible for such an isomer to remain in the ground state at finite temperature. For example, the 4A and 4B structures crossover at 720 K, 10A and 10B crossover at 390 K, and 10A and 10C crossover at 906 K. Also note that the theoretical transition temperature is not precise owing to the inherent limitation of DFT methodology.

C. Electronic properties

Fig. 5 presents the average lengths of the B–Si, Si–Si, and B–B bonds, Mayer bond order (MBO) and mean coordination number for the lowest-energy isomers of $B_3Si_n^-$ (n = 4–10) clusters. Usually, the bond length and coordination number of a cluster increase with the increasing number of atoms.[46] However, the variation trend here is not apparent for the $B_3Si_n^-$ clusters. Thus the B–B and B–Si bond lengths increase only slightly with the increasing number of atoms. The average B–B bond lengths in these low-energy structures are 1.72 Å, moderately shorter than those of B–Si (2.14 Å) and Si–Si (2.59 Å) bonds lengths, in accordance with Davy's[30] and Zhang's[33] results. The variation in bond lengths is in line with the analysis of Mayer bond order,[71] i.e., a shorter bond corresponds to a higher bond order. For example, the average MBO of B–B bonds in $B_3Si_4^-$ is 0.84 and it reduces to 0.66 for $B_3Si_5^-$, 0.63 for $B_3Si_6^-$, 0.54 for $B_3Si_7^-$, and 0.39 for $B_3Si_8^-$, respectively; then it increases to 0.54 for $B_3Si_9^-$ and 0.48 for $B_3Si_{10}^-$, respectively. Meanwhile, the MBO values of Si–Si bonds are 0.45 for $B_3Si_4^-$, 0.42 for $B_3Si_5^-$, 0.47 for $B_3Si_6^-$, 0.56 for $B_3Si_7^-$, and 0.34 for $B_3Si_8^-$, respectively; then it increases to 0.46 for $B_3Si_9^-$ and 0.37 for $B_3Si_{10}^-$, respectively. For a given $B_3Si_n^-$ cluster, the MBO value of B–Si bonds is larger than that of Si–Si bonds by about 0.14, suggesting stronger B–Si bonds with regard to Si–Si ones. Also note that there are local maxima at $B_3Si_9^-$ from the curves of Mayer bond order. Overall speaking, as the $B_3Si_n^-$ cluster grows, bond lengths slightly increase, the bond order becomes smaller, and the coordination number increases.

The relative stability of a $B_3Si_n^-$ cluster can be characterized by its binding energies (E_b) as follows:

$$E_b(\mathrm{B_3\,Si}_n{}^-) = [(n-1)E(\mathrm{Si}) + E(\mathrm{Si}^-) + 3E(\mathrm{B}) - E(\mathrm{B_3\,Si}_n{}^-)]\,/(n+3), \tag{2}$$

where $E(\mathrm{B})$, $E(\mathrm{Si})$, and $E(\mathrm{Si}^-)$ are the total energies of the neutral B atom, Si atom, and Si^- anion, respectively; $E(B_3Si_n^-)$ is the total energy of the anionic $B_3Si_n^-$ cluster. E_b as a function of cluster size is depicted in Fig. 6. A local maximum peak

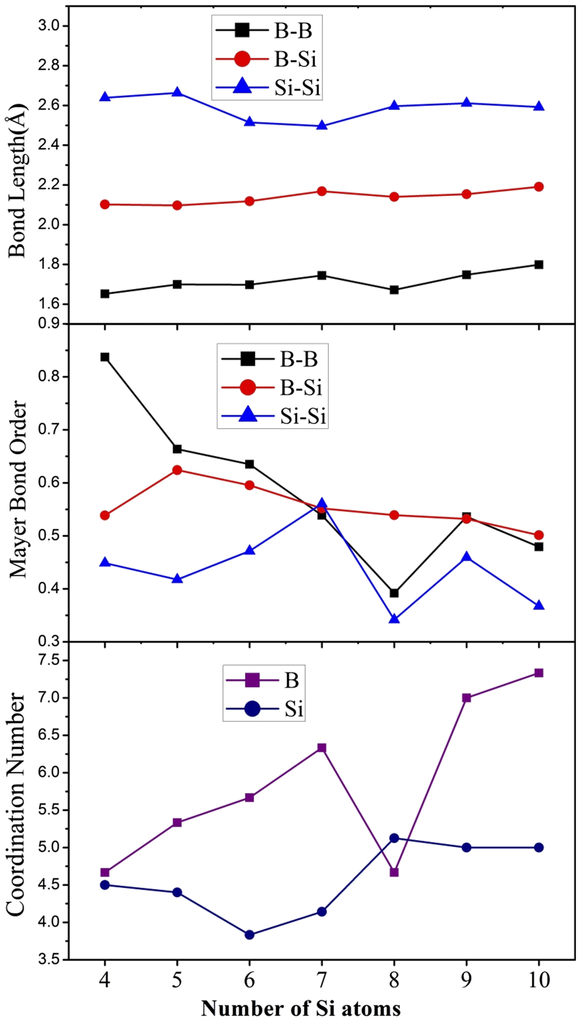

FIG. 5. Average B–B, B–Si, and Si–Si bond lengths, Mayer bond orders, and coordination number for the lowest energy isomers of $B_3Si_n^-$ (n = 4–10) cluster as a function of the number of Si atoms. The black squares, red dot lines, and blue triangles correspond to the B–B, B–Si, and Si–Si bond, respectively. Purple squares and navy blue dot line show the coordination numbers of B and Si, respectively. The cutoff radius of B–B, B–Si, and Si–Si bond is 1.80, 2.45, and 2.98 Å, respectively.

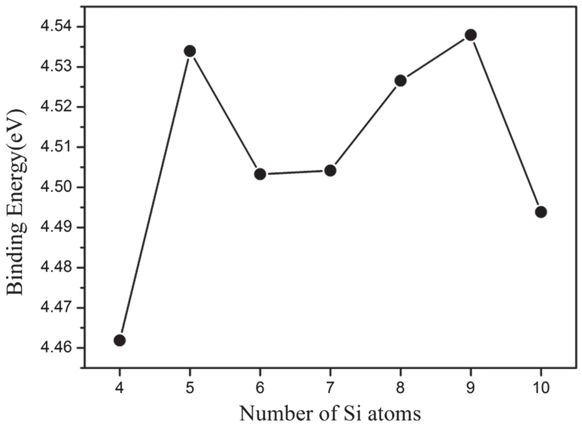

FIG. 6. The binding energies per atom (E_b) of the lowest-energy isomers of $B_3Si_n^-$ clusters anion at the B3LYP/6-311+G(d) level as function of the number of Si atoms.

is found for $B_3Si_n^-$ at n = 9, indicating the high stability of $B_3Si_9^-$. The HOMO-LUMO gaps of $B_3Si_n^-$ cluster anions calculated by B3LYP/6-311+G(d) method are summarized in Table I. Usually, the cluster with large HOMO–LUMO energy gap is highly stable against chemical reaction.[72,73] $B_3Si_9^-$ has a substantial gap of 3.18 eV, being one of the largest among the considered $B_3Si_n^-$. Combining the largest binding energy, very low VDE, and large HOMO-LUMO gap, we therefore suggest that the $B_3Si_9^-$ cluster anion is a highly stable species, which can be ascribed to a superatom cluster as discussed in Section III D.

In order to elucidate the evolution of electronic states in $B_3Si_n^-$ (n = 4–10) clusters, natural charge population (NCP) and natural electron configurations (NEC) for the lowest-energy structures of $B_3Si_n^-$ have been calculated and summarized in Table SII of the supplementary material. It can be clearly seen that the three boron atoms possess negative charges (0.54 to 1.46 e), which indicates the charge transfer from Si_n frame to B atoms, namely, boron acts as an electron acceptor in all $B_3Si_n^-$ clusters. This can be understood by the electronegativities of these two elements: 2.04 for B and 1.90 for Si in Pauli scale. According to Table SII, both interatomic electron transfer from 3*s* orbital of Si to B and intra-atomic electron transfer from 2*s* orbital of B to 2*p* orbital result in a nearly $2s^1 2p^3$ electronic configuration in the B atoms, which indicates strong *s*–*p* hybridization in the B atoms of $B_3Si_n^-$ clusters. The partial density of states (PDOS) of $B_3Si_4^-$ and $B_3Si_9^-$ clusters shown in Fig. S2 of the supplementary material further demonstrates strong coupling between B atoms and Si atoms. Specifically, the 2*p* states in every boron atom gain 1.57–2.46 electrons, while 2*s* orbital loses 0.90–1.16 electrons, respectively. As cluster size increases, the population of 2*s* orbital of boron nearly remains the same value (around 0.91 electrons), while the number of electrons on 2*p* orbital of boron gradually increases from 2.57 to 3.46 electrons.

D. $B_3Si_9^-$ as a superatom cluster

From the above discussions of $B_3Si_n^-$ clusters, $B_3Si_9^-$ with high symmetry (C_{3v}), enhanced bond order, low VDE, large HOMO-LUMO gap, and binding energy stands out as a highly stable species. The unusual stability of $B_3Si_9^-$ can be interpreted by the concept of "superatom." Generally speaking, the electronic states in a superatom cluster are delocalized over the entire cluster with spatial shapes resembling the atomic orbitals. The corresponding energy eigenvalues can be grouped into atomic-like shells (1S, 1P, 1D, 2S, 2P, 1F, etc.), depending on the degeneracy and spatial symmetry of the molecular orbitals.[74,75]

The energy levels and spatial distribution of the occupied molecular orbitals of $B_3Si_9^-$ in its ground state geometry are shown in Fig. 7. There are totally 46 electrons: 6 electrons being localized on the three B–B bonds and the rest 40 electrons acting as skeletal electrons. This conjecture is supported by the plot of molecular orbitals in Fig. 7, in which one can clearly see the atomic-orbital-like feature for the 1S, 1P, 1D, 2S, 2P, 1F superatom orbitals and three additional molecular orbitals mainly localized on the B–B bonds with C_{3v} symmetry. Due to the C_{3v} symmetry of cluster, these superatom orbitals deviate from perfect spherical harmonics.

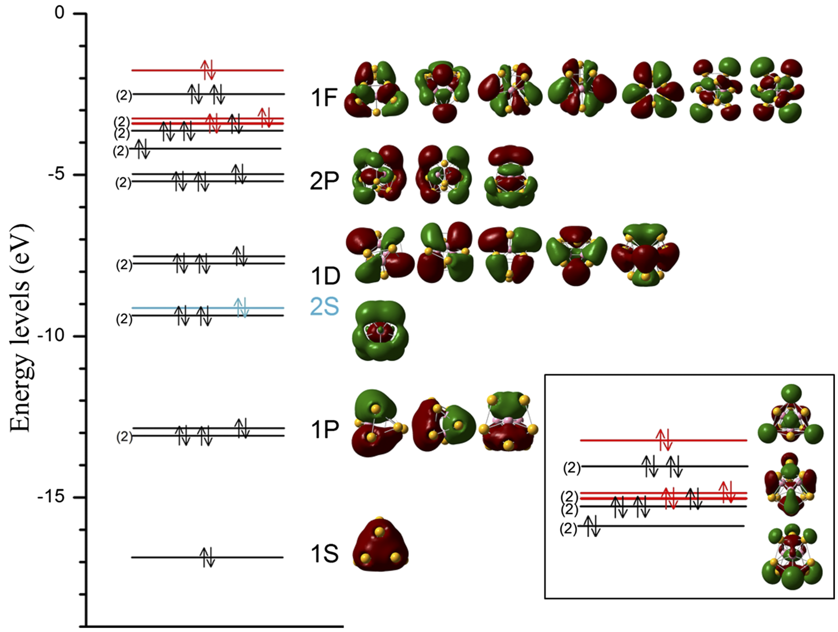

FIG. 7. Energy levels (left) and the occupied superatom orbitals (right) for the $B_3Si_9^-$ cluster. The red arrows are the six electrons for B–B bonds and the blue arrows are the energy level of 2S which is mixed with the energy levels of 1D. The three additional molecular orbitals localized on the B–B bonds are shown in the inset plot (right lower).

Note that the 40 skeletal electrons corresponding to molecular orbital configuration of $1S^2 1P^6 1D^{10} 2S^2 2P^6 1F^{14}$ are the magic number of closed electron shell within the jellium model (JSM).[76] Previously, many other superatom clusters with 40 skeletal electrons, such as Al_{13}^-[77] and $[As@Ni_{12}@As_{20}]$,[3–78] have already been found. Although $B_3Si_9^-$ has a total of 46 valence electrons, our result indicates that the total number of valence electrons in a superatom cluster is not necessary to coincide with the magic number of closed electron shell, if one has taken into account some extra electrons localized on some particular bonds. The present finding of $B_3Si_9^-$ has not only enriched the family of superatom clusters but also extended the scope of them.

IV. CONCLUSIONS

A systematic investigation on the low-lying structures, growth behavior, relative stabilities, and electronic properties of the $B_3Si_n^-$ (n = 4–10) clusters have been performed using DFT calculations at the B3LYP/6-311+G(d) level of theory, combined with experimental anion photoelectron spectroscopy. The good agreement between the experimental photoelectron spectra and the simulated ones proves the validity of our calculations. Our major finding can be summarized as follows:

(1) The lowest-energy structures of $B_3Si_n^-$ (n = 4–10) clusters favor close deltahedra up to 13 vertices with the central squashed pentagonal bipyramid (4A structure) as a building unit. The boron atoms tend to bond with each other forming B_3 triangle with stronger B–B bonds than B–Si bonds. Meanwhile, boron atoms prefer occupying vertices of relatively low curvature or even negative curvature.

(2) The analysis of natural population and partial density of states show the electrons transfer from 3*s* orbital of silicon and 2*s* orbital of boron to 2*p* orbital of boron as well as strong *s*-*p* hybridization in these $B_3Si_n^-$ clusters.

(3) From the size-dependence of binding energies, ADEs and VDEs, HOMO–LUMO gaps, and Mayer bond orders of $B_3Si_n^-$ (n = 4–10) clusters, the $B_3Si_9^-$ cluster with C_{3v} symmetry exhibits relatively higher stability. This can be well explained by the picture of superatom with a magic number of 40 skeletal electrons and a closed-shell molecular orbital configuration of $1S^2 1P^6 1D^{10} 2S^2 2P^6 1F^{14}$.

SUPPLEMENTARY MATERIAL

See supplementary material for the electronic properties and the free energy of $B_3Si_n^-$ (n = 4–10) clusters.

ACKNOWLEDGMENTS

This work was supported by the National Natural Science Foundation of China (Nos. 11574040, 11604039, 21103202, and 11374045), the Fundamental Research Funds for the Central Universities of China (Nos. DUT16LAB01 and DUT15RC(3)099), the Chinese Academy of Sciences (Grant No. QYZDB-SSW-SLH024) and the Supercomputing Center of Dalian University of Technology.

[1] X. Zhu and X. C. Zeng, J. Chem. Phys. **118**, 3558 (2003).
[2] X. Zhu, X. C. Zeng, Y. Lei, and B. Pan, J. Chem. Phys. **120**, 8985 (2004).
[3] S. Yoo and X. C. Zeng, J. Chem. Phys. **124**, 054304 (2006).
[4] S. Yoo and X. C. Zeng, Angew. Chem. **117**, 1515 (2005).
[5] S. Yoo, J. Zhao, J. Wang, and X. C. Zeng, J. Am. Chem. Soc. **126**, 13845 (2004).
[6] L. Ma, J. Zhao, J. Wang, B. Wang, and G. Wang, Phys. Rev. A **73**, 063203 (2006).
[7] S. Yoo, N. Shao, C. Koehler, T. Fraunhaum, and X. C. Zeng, J. Chem. Phys. **124**, 164311 (2006).
[8] V. Kumar and Y. Kawazoe, Phys. Rev. Lett. **87**, 045503 (2001).
[9] A. K. Singh, V. Kumar, T. M. Briere, and Y. Kawazoe, Nano Lett. **2**, 1243 (2002).
[10] V. Kumar and Y. Kawazoe, Phys. Rev. B **65**, 125403 (2002).
[11] P. Guo, Z. Y. Ren, F. Wang, J. Bian, J. G. Han, and G. H. Wang, J. Chem. Phys. **121**, 12265 (2004).

[12] A. P. Yang, Z. Y. Ren, P. Guo, and G. H. Wang, J. Mol. Struct.: THEOCHEM **856**, 88 (2008).

[13] L. Sai, L. Tang, J. Zhao, J. Wang, and V. Kumar, J. Chem. Phys. **135**, 184305 (2011).

[14] X. Huang, H.-G. Xu, S. Lu, Y. Su, R. King, J. Zhao, and W. Zheng, Nanoscale **6**, 14617 (2014).

[15] J. Zhao, R. Shi, L. Sai, X. Huang, and Y. Su, Mol. Simul. **42**, 809 (2016).

[16] W. Zheng, J. M. Nilles, D. Radisic, and K. H. Bowen, J. Chem. Phys. **122**, 071101 (2005).

[17] H. G. Xu, Z. G. Zhang, Y. Feng, J. Yuan, Y. Zhao, and W. Zheng, Chem. Phys. Lett. **487**, 204 (2010).

[18] H. G. Xu, Z. G. Zhang, Y. Feng and W. Zheng, Chem. Phys. Lett. **498**, 22 (2010).

[19] H. G. Xu, M. M. Wu, Z. G. Zhang, Q. Sun, and W. J. Zheng, Chin. Phys. B **20**, 043102 (2011).

[20] X. Kong, H. G. Xu, and W. Zheng, J. Chem. Phys. **137**, 064307 (2012).

[21] H. G. Xu, M. M. Wu, Z. G. Zhang, J. Yuan, Q. Sun, and W. Zheng, J. Chem. Phys. **136**, 104308 (2012).

[22] X. H. Li, J. Carlsson, M. Johansson, B. Ekström, S. Gong, and H. Hentzell, Appl. Phys. Lett. **61**, 1316 (1992).

[23] D. De Salvador, G. Bisognin, M. Di Marino, E. Napolitani, A. Carnera, S. Mirabella, E. Pecora, E. Bruno, F. Priolo, and H. Graoui, J. Vac. Sci. Technol., B **26**, 382 (2008).

[24] J. Yamauchi, N. Aoki, and I. Mizushima, Phys. Rev. B **55**, 10245 (1997).

[25] A. Poyai, E. Simoen, and C. Claeys, Appl. Phys. Lett. **78**, 949 (2001).

[26] J. Yamauchi, Y. Yoshimoto, and Y. Suwa, Appl. Phys. Lett. **99**, 191901 (2011).

[27] K. Ohmori, N. Esashi, M. Takao, D. Sato, and Y. Hayafuji, Appl. Phys. Lett. **87**, 112101 (2005).

[28] O. CojocaruMirédin, D. Mangelinck, and D. Blavette, J. Appl. Phys. **106**, 113525 (2010).

[29] A. I. Boldyrev and J. Simons, J. Phys. Chem. **97**, 1526 (1993).

[30] R. Davy, E. Skoumbourdis, and D. Dinsmore, Mol. Phys. **103**, 611 (2005).

[31] L. T. Ueno, V. O. Kiohara, L. F. Ferrão, M. Pelegrini, O. Roberto-Neto, and F. B. Machado, J. Mol. Model. **21**, 1 (2015).

[32] V. T. Ngan and M. T. Nguyen, J. Phys. Chem. A **114**, 7609 (2010).

[33] Z. Sun, Z. Yang, Z. Gao, and Z. Tang, Rapid Commun. Mass Spectrom. **21**, 792 (2007).

[34] T. B. Tai, P. Kadłubański, S. Roszak, D. Majumdar, J. Leszczynski, and M. T. Nguyen, ChemPhysChem **12**, 2948 (2011).

[35] N. M. Tam, T. B. Tai, and M. T. Nguyen, J. Phys. Chem. C **116**, 20086 (2012).

[36] L. B. Knight, Jr., A. J. McKinley, R. M. Babb, M. D. Morse, and C. A. Arrington, J. Chem. Phys. **98**, 6749 (1993).

[37] N. X. Truong, M. Haertelt, B. K. Jaeger, S. Gewinner, W. Schöllkopf, A. Fielicke, and O. Dopfer, Int. J. Mass spectrom. **395**, 1 (2016).

[38] G. J. Cao, S. J. Lu, H. G. Xu, X. L. Xu, and W. J. Zheng, RSC Adv. **6**, 62165 (2016).

[39] D. M. Deaven and K. M. Ho, Phys. Rev. Lett. **75**, 288 (1995).

[40] J. Zhao and R. H. Xie, J. Comput. Theor. Nanosci. **1**, 117 (2004).

[41] L. Sai, J. Zhao, X. Huang, and J. Wang, J. Nanosci. Nanotechnol. **12**, 132 (2012).

[42] X. Huang, L. Sai, X. Jiang, and J. Zhao, Eur. Phys. J. D **67**, 43 (2013).

[43] X. Liang, X. Huang, Y. Su, and J. Zhao, Chem. Phys. Lett. **634**, 255 (2015).

[44] X. Huang, S.-J. Lu, X. Liang, Y. Su, L. Sai, Z.-G. Zhang, J. Zhao, H.-G. Xu, and W. Zheng, J. Phys. Chem. C **119**, 10987 (2015).

[45] L. Sai, L. Tang, X. Huang, G. Chen, J. Zhao, and J. Wang, Chem. Phys. Lett. **544**, 7 (2012).

[46] X. Huang, Y. Su, L. Sai, J. Zhao, and V. Kumar, J. Cluster Sci. **26**, 389 (2015).

[47] L. Hong, H. Wang, J. Cheng, X. Huang, L. Sai, and J. Zhao, Comput. Theor. Chem. **993**, 36 (2012).

[48] J. P. Perdew, K. Burke, and M. Ernzerhof, Phys. Rev. Lett. **77**, 3865 (1996).

[49] B. Delley, J. Chem. Phys. **92**, 508 (1990).

[50] B. Delley, J. Chem. Phys. **113**, 7756 (2000).

[51] C. Lee, W. Yang, and R. G. Parr, Phys. Rev. B **37**, 785 (1988).

[52] A. D. Becke, J. Chem. Phys. **98**, 5648 (1993).

[53] M. J. Frisch, G. W. Trucks, H. B. Schlegel *et al.*, Gaussian 09, Revision A.01, Gaussian Inc., Wallingford, CT, 2009.

[54] J. A. Kerr, Anal. Chim. Acta **144**, 298 (1982).

[55] A. D. J. Becke, J. Chem. Phys. **88**, 2547 (1988).

[56] J. P. Perdew and Y. Wang, Phys. Rev. B **45**, 13244 (1992).

[57] A. E. Reed and F. Weinhold, J. Chem. Phys. **78**, 4066 (1983).

[58] A. E. Reed and F. Weinhold, J. Chem. Phys. **83**, 1736 (1985).

[59] A. E. Reed, R. B. Weinstock, and F. Weinhold, J. Chem. Phys. **83**, 735 (1985).

[60] A. E. Reed, L. A. Curtiss, and F. Weinhold, Chem. Rev. **88**, 899 (1988).

[61] J. E. Carpenter and F. Weinhold, J. Mol. Struct.: THEOCHEM **169**, 41 (1988).

[62] L. S. Wang, H. S. Cheng, and J. Fan, J. Chem. Phys. **102**, 9480 (1995).

[63] D. J. Tozer and N. C. Handy, J. Chem. Phys. **109**, 10180 (1998).

[64] J. Akola, M. Manninen, H. Häkkinen, U. Landman, X. Li, and L.-S. Wang, Phys. Rev. B **60**, 11297 (1999).

[65] K. Wade, Chem. Commun. **15**, 792 (1971).

[66] D. M. P. Mingos, Acc. Chem. Res. **17**, 311 (1984).

[67] J. Aihara, J. Am. Chem. Soc. **100**, 3339 (1978).

[68] R. King and D. Rouvray, J. Am. Chem. Soc. **99**, 7834 (1977).

[69] R. B. King, Chem. Rev. **101**, 1119 (2001).

[70] R. King, Inorg. Chem. **45**, 8211 (2006).

[71] I. Mayer, Int. J. Quantum Chem. **29**, 477 (1986).

[72] J. Li, X. Li, H.-J. Zhai, and L.-S. Wang, Science **299**, 864 (2003).

[73] H. Kawamura, V. Kumar, and Y. Kawazoe, Phys. Rev. B **70**, 245433 (2004).

[74] A. W. Castleman and S. N. Khanna, J. Phys. Chem. C **113**, 2664 (2009).

[75] P. Jena, J. Phys. Chem. Lett. **4**, 1432 (2013).

[76] M. Brack, Rev. Mod. Phys. **65**, 677 (1993).

[77] D. E. Bergeron, A. W. Castleman, T. Morisato, and S. N. Khanna, Science **35**, 84 (2004).

[78] R. B. King and J. Zhao, Chem. Commun. **38**, 4204 (2006).